Received July 29, 2019, accepted August 16, 2019, date of publication August 28, 2019, date of current version September 12, 2019.

Digital Object Identifier 10.1109/ACCESS.2019.2937945

Experimental Verification of Human Body Communication Path Gain Channel Modeling for Muscular-Tissue Characteristics

SHUANG ZHANG[1,2,3,4,5,6,7], (Senior Member, IEEE), YI HE LIU[1,7], (Member, IEEE), YU PING QIN[1,7], JIANG MING KUANG[1,7], JI NING YANG[1,7], JIA WEN LI[5,6], (Member, IEEE), JIU JIANG WANG[1,5,6,7], (Senior Member, IEEE), TAO ZHANG[2,3,4], AND XUE MING ZOU[2,3,4]

[1]Data Recovery Key Laboratory of Sichuan Province, College of Computer Science and AI, Neijiang Normal University, Neijiang 641100, China
[2]School of Life Science and Technology, University of Electronic Science and Technology of China, Chengdu 611731, China
[3]High Field Magnetic Resonance Brain Imaging Laboratory of Sichuan, Chengdu 611731, China
[4]Key Laboratory for NeuroInformation of Ministry of Education, School of Life Science and Technology, University of Electronic Science and Technology of China, Chengdu 611731, China
[5]State Key Laboratory of Analog and Mixed-Signal VLSI, University of Macau, Macau 999078, China
[6]Department of Electrical and Computer Engineering, Faculty of Science and Technology, University of Macau, Macau 999078, China
[7]BeiDou and Wisdom Medical Doctor Workstation, Neijiang Normal University, Neijiang 641110, China

Corresponding authors: Jiu Jiang Wang (tswangjade@gmail.com) and Tao Zhang (taozhangjin@gmail.com)

This work was supported in part by the Leading Talent Training Project of Neijiang Normal University under Grant 2017[Liu Yi-He], in part by the Innovative Team Program of Neijiang Normal University under Grant 17TD03, in part by the Foundation of Ph.D. Scientific Research of Neijiang Normal University under Grant RSC201704, in part by the Sichuan Science and Technology Program under Grant 2019YJ0181, in part by the Sichuan Province Academic and Technical Leader Training Funded Projects under Grant 13XSJS002, in part by the National Key Research and Development Program of China under Grant 2016YFC0100800 and Grant 2016YFC0100802, and in part by the Foundation of Ph.D. Scientific Research of Neijiang Normal University under Grant 2019[zhang shuang] and Grant 2019[wang jiujiang].

ABSTRACT To study the signal transmission mechanism in the human body, the channel characteristics are generally analyzed by modeling. In current modeling methods, the human body is considered quasi-static and the human tissues isotropic, for simplifying the model and its calculation; however, this does not consider the effect of the human tissues on electric signal transmission, resulting in considerable deviations between the calculated results and the measured values. To reduce model errors and improve precision, a channel modeling method with human muscular-tissue characteristics is proposed in this study. In this method, Maxwell's equations is used as the governing equation and a galvanic-coupling intra-body communication channel model with human-tissue characteristics is built in the cylindrical coordinate system. By building a numerical model with the same parameters as in the analytical model, the analytical solution is proved to be correct. By comparing the different-sample anisotropic models and the isotropic models with the experimental results, it is concluded that the anisotropic model with muscular-tissue characteristics is superior to the isotropic model without muscular-tissue characteristics, with respect to the curve variation tendency and error between the model calculations and the experimental results. The precision of this anisotropic model is enhanced by 200%; hence, it is more accurate. At last, in order to study the optimal communication frequency of the channel, we select 50 healthy persons as the subjects of this experiment, we find that the optimal communication frequency band of the human arm is 10 kHz to 50 kHz. Within this frequency band, the channel gain is the largest, and the mean deviation of samples is less than 2dB, which is very beneficial to signal transmission in human body.

INDEX TERMS Tissue characteristics, galvanic coupling, human-body communication, channel modeling.

I. INTRODUCTION

A Body area network (BAN) consists of node devices distributed on the surface of the human body or implanted in the human body; signals are transmitted around and inside the human body through specific communication paths. Devices distributed on the surface of the human body such as for the electrocardiogram [1], temperature [2], heart rate [3]–[5], and blood pressure [6], [7], are generally called wearable

The associate editor coordinating the review of this article and approving it for publication was Nuno Garcia.

devices and are used to monitor human physiological signals by physical contact. The implantable sensors are called implantable devices. Among the current implantable devices, in addition to smart pills for precision drug delivery [8], glucose monitoring [8] and eye pressure sensing systems [9], the cardiac pacemaker is the most successful and most widely used product [10]. For building a good BAN working environment, it is necessary to select an appropriate communication method to achieve data communication. Currently, there are two methods for data communication, wired and wireless. In wired communication, connected wires are used to connect all node equipment for data transmission. Although in this method the communication is steady and fast, owing to wiring, networking is complicated and human body movement introduces noise easily. Particularly, in implantable communication, wiring causes infection; hence, wire communication is not generally used in networking. The other method is wireless communication, which includes electromagnetic coupling [11], radio frequency communication [12], [13], and human-body communication [14]–[24]. Electromagnetic coupling and radio frequency methods have wide bandwidths, fast communication speeds, and steady communication but they require a high communication frequency, have poor signal control, weak anti-interference performance, and large signal attenuation; therefore, they are unsuitable for networking. For implantable medical facilities with communication frequencies below 1 MHz, in particular, electromagnetic coupling and radio frequency methods have no advantages.

Intra-body communication technology [14]–[24] is an important data communication method in modern medical monitoring and measuring. Human tissues are used as the communication media and signals are transmitted through them; hence, complicated wiring is avoided when establishing the body area network. In addition, as a communication antenna is not required for sending and receiving signals, in the implantable-device design process, the signal antenna need not be considered, reducing injury to human tissue. Therefore, it is significant in future medical monitoring and measurement [25].

Galvanic-coupling human-body communication is a human-body communication method in which the human body is regarded as a resistor; the signal is input to the human tissues in the form of a current [26] and freely transmitted through the human tissues. In this method, as it is not necessary to form a loop with the environment ground, it is more suitable for communication in implantable medical equipment. Currently, research on galvanic-coupling human-body communication technology is still nascent; there are few studies on the effect of volume-conductor tissue characteristics on the channel, in particular. In order to explain the signal distribution in the human tissue, for model simplification, human tissue (skeleton, muscle, fat and skin) is regarded as a volume conductor [26]–[31] and considered to be isotropic; the channel model is built based on the volume conductor theory and Maxwell's equations [20], [29]–[32]. However, this ignores the effect of the tissue characteristics on the channel. Several experiments demonstrate that human tissue is not completely isotropic. Because of the difference between the parallel and the transverse growth characteristics of some tissues, the parallel electric characteristics differ considerably from the transverse [32]–[35].

The main contributions of this paper are given as follows:

- 1) The transverse and the parallel characteristics of muscle fiber tissue are added into the analytical solution model to make the model closer to the real experimental environment;
- 2) The consistency between the model results and the experimental results is verified by several sample experiments;
- 3) The best communication range of the forearm is found by analyzing the experimental sample data, this lays the foundation for the design of the communication system.

In this paper, the authors propose an analytical model with multilayer of anisotropic tissues, which is fast solving and has high repeatability; but existing intra-body communication models don't posses these properties. Meanwhile, the performance of the model is verified by a large number of experiments. Section I introduces the research background and purpose. Section II presents the research method including the structure of the fiber and the modeling methods. Section III details the experimental verification, in which a series of experiments are conducted to verify the accuracy and rationality of the model. Section IV presents the best communication bandwidth for communication channel. Section V discusses some of the limitations affecting the results obtained in Sections II, III and IV, Section VI presents some future works and Section VII concludes the work.

II. METHODS

A. STRUCTURE OF THE FIBERS

On the basis of Gielen's study [34], we know that muscle tissue is made up of muscle fibers (Figure 1). In the growth process of muscle fibers, due to difference growth characteristics in parallel and transverse directions, they are also significantly different in electrical characteristics:

- Conductivity parallel to the muscle fibres (σ_l) [34]:

$$0.33 < \sigma_l < 0.80(\Omega m)^{-1}. \quad (1)$$

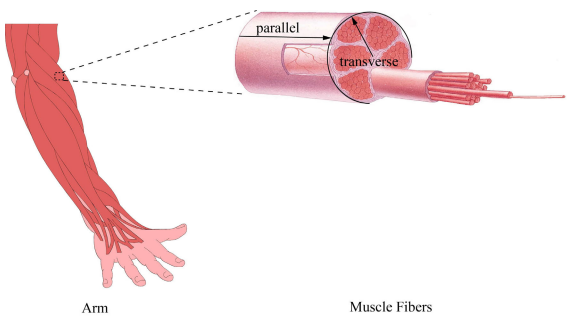

FIGURE 1. The arm fibers structure.

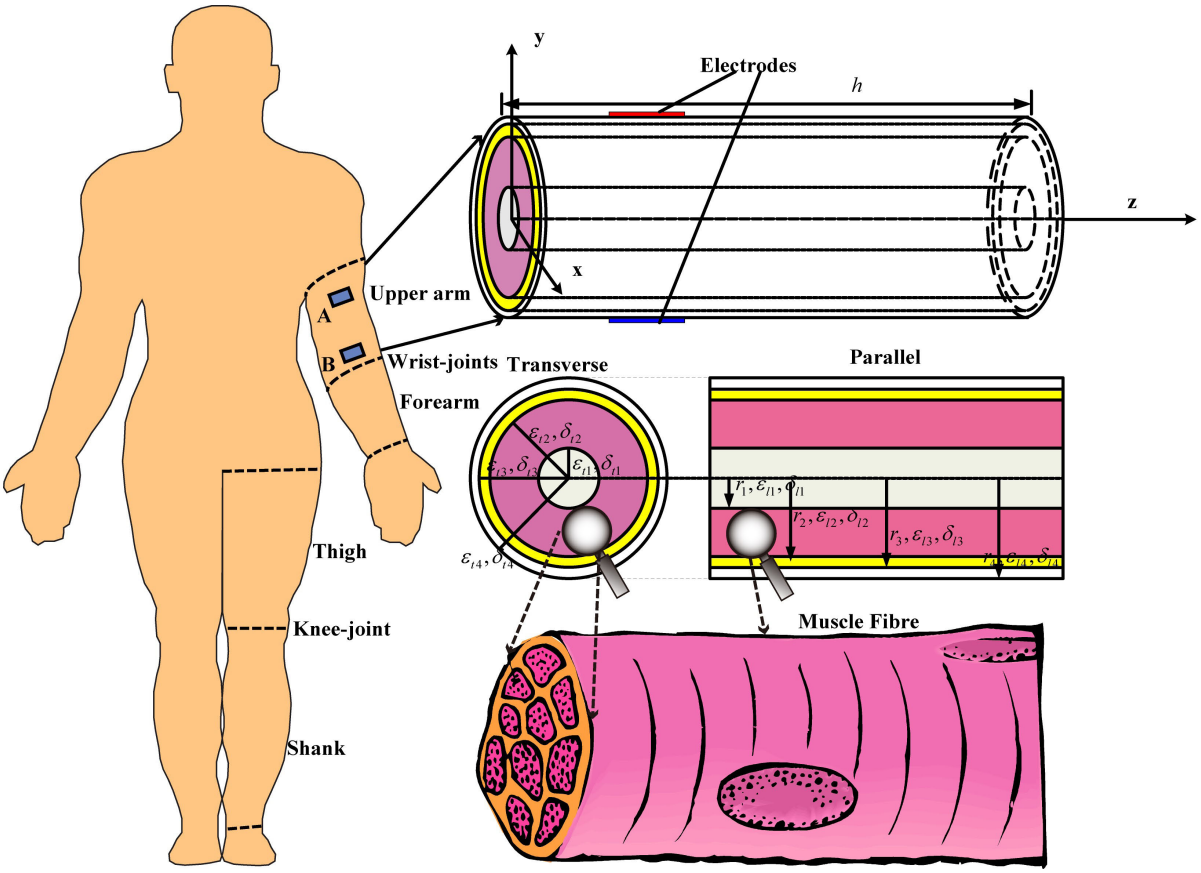

FIGURE 2. Equivalent multilayer geometric model of the human arms.

- Conductivity transverse to the muscle fibres (σ_t) [34]:

$$0.03 < \sigma_t < 0.15(\Omega m)^{-1}. \tag{2}$$

- Anisotropy ratio $\frac{\sigma_l}{\sigma_t}$ [34]:

$$2.04 < \frac{\sigma_l}{\sigma_t} < 26.67. \tag{3}$$

Because we mainly study the influence of the conductivity on the channel along transverse and parallel directions of muscle fibers, we obtain the matrix of the muscle layer with the conductivity characteristics in the frequency domain:

$$\widetilde{\sigma}(f) = \begin{bmatrix} \widetilde{\sigma}_t(f) & 0 & 0 \\ 0 & \widetilde{\sigma}_t(f) & 0 \\ 0 & 0 & \widetilde{\sigma}_l(f) \end{bmatrix} \tag{4}$$

Next, let's do the coordinate transformation:

$$x' = \frac{\widetilde{\sigma}_t}{\sqrt{\widetilde{\sigma}_t \widetilde{\sigma}_l}} x \tag{5}$$

$$y' = \frac{\widetilde{\sigma}_t}{\sqrt{\widetilde{\sigma}_t \widetilde{\sigma}_l}} y \tag{6}$$

$$z' = \frac{\widetilde{\sigma}_l}{\sqrt{\widetilde{\sigma}_t \widetilde{\sigma}_l}} z \tag{7}$$

Therefore, in the new coordinate system, the potential distribution can be expressed as follows:

$$\varphi'(x', y', z') = \varphi(x, y, z) \tag{8}$$

Next we will continue to complete the channel modeling in the new coordinate system.

B. MATHEMATICAL MODEL

Based on the previous research results, human limbs are first abstracted as standard multilayer cylindrical structures in galvanic coupling human-body communication; two pairs of electrodes are used as the signal transmitting and receiving terminals, respectively, as depicted in Figure 2. Human limbs with lengths h is equivalent to a multilayered concentric cylinder with skeleton, muscle, fat, and skin structures. According to the anatomical characteristics, $(r_1, r_2, \cdots, r_{N-1}, r_N)$ are the circumscribed radii of all the tissues on the tangent plane, where N is the outermost layer. $(\varepsilon_{t1}, \varepsilon_{t2}, \cdots, \varepsilon_{t(N-1)}, \varepsilon_{tN})$ and $(\varepsilon_{l1}, \varepsilon_{l2}, \cdots, \varepsilon_{l(N-1)}, \varepsilon_{lN})$ represent the transverse and parallel dielectric constants, respectively, of all tissues, $(\sigma_{t1}, \sigma_{t2}, \cdots, \sigma_{t(N-1)}, \sigma_{tN})$ and $(\sigma_{l1}, \sigma_{l2}, \cdots, \sigma_{l(N-1)}, \sigma_{lN})$, respectively, are the transverse and parallel conductivities of all the tissues [36].

Under the quasi-static condition from [37], [38], the electric potential distribution of the volume conductor may be expressed as

$$\nabla \cdot \widetilde{\sigma}_s \nabla \varphi \approx 0, \quad s = 1, 2, \cdots, N-1, N \tag{9}$$

where φ is the interior electric potential in the human-limb tissue. $\widetilde{\sigma_s}$ is the combination conductivity of the tissue in the *s-th* layer at a frequency f and is expressed as follows:

$$\widetilde{\sigma}_s = \sqrt{\widetilde{\sigma}_{ts}(f)\widetilde{\sigma}_{ls}(f)}, \quad s = 1, 2, \cdots, N-1, N \tag{10}$$

Note that $\widetilde{\sigma}_{ts}(f)$ and $\widetilde{\sigma}_{ls}(f)$ are, respectively, the parallel and transverse composite electric conductivities of the tissue in the *s-th* layer at a frequency f and is expressed as follows:

$$\widetilde{\sigma}_{ts}(f) = \sigma_{ts}(f) + j\omega\varepsilon_{ts}(f)\varepsilon_0, \quad s = 1, 2, \cdots, N-1, N \tag{11}$$
$$\widetilde{\sigma}_{ls}(f) = \sigma_{ls}(f) + j\omega\varepsilon_{ls}(f)\varepsilon_0, \quad s = 1, 2, \cdots, N-1, N \tag{12}$$

where $\sigma_{ts}(f)$ and $\sigma_{ls}(f)$ indicate the transverse and the parallel conductivity of the tissue in the *s-th* layer at a frequency f, respectively; $\varepsilon_{ts}(f)$ and $\varepsilon_{ls}(f)$ indicate the transverse and the parallel relative dielectric constants of the tissue in the tissue in the *s-th* layer at a frequency f, respectively and ε_0 is the dielectric constant in vacuum.

Based on the cylindrical coordinate transformation relationship between muscle-fiber anisotropy and tissue isotropy, the following can be derived [36]:

$$\nabla^2\varphi^*(r^*, \theta, z^*) \approx 0 \tag{13}$$

and

$$\varphi^*(r^*, \theta, z^*) = \varphi(r, \theta, z) \tag{14}$$

where $r^* = \sqrt{\widetilde{\sigma}_{ts}(f)/\widetilde{\sigma}_s(f)}r$ and $z^* = \sqrt{\widetilde{\sigma}_{ls}(f)/\widetilde{\sigma}_s(f)}z$

C. BOUNDARY AND CONTINUITY CONDITIONS

In order to derive the model solution in a volume conductor, the model should satisfy the boundary conditions, (16) and(18), presented in this section.

$$\widetilde{\sigma}_{tN}(f)\frac{\partial\varphi(f, r, \theta, z)}{\partial r}\Big|_{r=r_N} = \vec{J}_{nt}(f, \theta, z) \tag{15}$$
$$\vec{J}_{nt}(f, {r_s}^+, z) = \vec{J}_{nt}(f, {r_s}^-, z) \tag{16}$$
$$\varphi_s({r_s}^+, z) = \varphi_s({r_s}^-, z) \tag{17}$$
$$\widetilde{\sigma}_{ts}(f)\frac{\partial\varphi(f, {r_s}^+, \theta, z)}{\partial r} = \widetilde{\sigma}_{t(s+1)}(f)\frac{\partial\varphi(f, {r_s}^-, \theta, z)}{\partial r} \tag{18}$$

And assumption:

$$\varphi(r, \theta, z)\mid_{z=0} = \varphi(r, \theta, z)\mid_{z=h} = 0 \tag{19}$$

where $\vec{J}_{nt}(f, \theta, z)$ depicts the normal component of the current density applied to the limb through the side surfaces.

D. POTENTIAL DISTRIBUTION MODEL

In combination with the quasi-static approximation electromagnetic boundary conditions [37] and the Laplace's anisotropic tissue equation in the cylindrical coordinate system [38]–[40], a variable separation approach is used to derive the electric potential distribution of all the layers of human forearm tissue at a frequency f, which can be expressed as follows [41]:

$$\begin{aligned}\varphi_{sL}(f, r, \theta, z)_{Anisotropic} &= \sum_{s=1}^{\infty}\sum_{m=1}^{\infty}\sum_{n=1}^{\infty}[A_{sL}(f)I_n(\frac{m\pi r}{h}\sqrt{\widetilde{\sigma}_s(f)/\widetilde{\sigma}_{ts}(f)}) \\ &+ B_{sL}(f)K_n(\frac{m\pi r}{h}\sqrt{\widetilde{\sigma}_s(f)/\widetilde{\sigma}_{ts}(f)})][C_{sL}(f)cos(n\theta) \\ &+ D_{sL}(f)sin(n\theta)]sin(\frac{m\pi z}{h}\sqrt{\widetilde{\sigma}_s(f)/\widetilde{\sigma}_{ls}(f)}) \\ &\quad s = 1, 2, \cdots, N-1, N\end{aligned} \tag{20}$$

where $I_n(\,)$is the *n-th* order modified Bessel function of the first kind and $K_n(\,)$ is the *n-th* order modified Bessel function of the second kind [20], [30], [31]; $A_{sL}(f)$, $B_{sL}(f)$, $C_{sL}(f)$ and $D_{sL}(f)$ indicate constant coefficients of the electric potential equation concerning the tissue in the *s*-th layer at a frequency f.

When $\widetilde{\sigma}_s = \widetilde{\sigma}_{ts}(f) = \widetilde{\sigma}_{ls}(f)$ is true, the tissue characteristics in all the directions are identical at a frequency f; hence, the electric potential equation of the isotropic tissue in the cylindrical coordinate system can be obtained as follows:

$$\begin{aligned}\varphi_{sL}(f, r, \theta, z)_{Isotropic} &= \sum_{s=1}^{\infty}\sum_{m=1}^{\infty}\sum_{n=1}^{\infty}[A_{sL}(f)I_n(\frac{m\pi r}{h}) + B_{sL}(f)K_n(\frac{m\pi r}{h})] \\ &\times[C_{sL}(f)cos(n\theta) + D_{sL}(f)sin(n\theta)]sin(\frac{m\pi z}{h}) \\ &\quad s = 1, 2, \cdots, N-1, N\end{aligned} \tag{21}$$

This corresponds to the conclusion drawn by X. M. CHEN etc. [30], where the tissue is isotropic in the frequency domain.

For better understanding of the proposed model, the model calculation flow chart is summarized as in Figure 3.

E. PATH-GAIN MODEL

From potential distribution model, the path gain *PG* model can be expressed as:

$$\begin{aligned}G(f, r, \theta, z)\mid_{dB} &= 20log_{10}(\frac{\varphi_{RX}(f, r, \theta, z)}{\varphi_{TX}(f, r_0, \theta, z_0)}) \\ &= 20log_{10}(R(f, r)) + 20log_{10}(\Phi(f, \theta)) \\ &\quad + 20log_{10}(Z(f, z)) - 20log_{10}(\varphi_{source}(f, r_0, \theta, z_0)))\end{aligned} \tag{22}$$

where

$$\begin{aligned}R(f, r) = \sum_{s=1}^{N}\sum_{m=1}^{\infty}\sum_{n=1}^{\infty}[[A_{sL}(f)I_n(\frac{m\pi r}{h}\sqrt{\widetilde{\sigma}_s(f)/\widetilde{\sigma}_{ts}(f)}) \\ + B_{sL}(f)K_n(\frac{m\pi r}{h}\sqrt{\widetilde{\sigma}_s(f)/\widetilde{\sigma}_{ts}(f)})];\end{aligned} \tag{23}$$

$$\Phi(f, \theta) = \sum_{n=1}^{\infty}[C_{sL}(f)cos(n\theta) + D_{sL}(f)sin(n\theta)]; \tag{24}$$

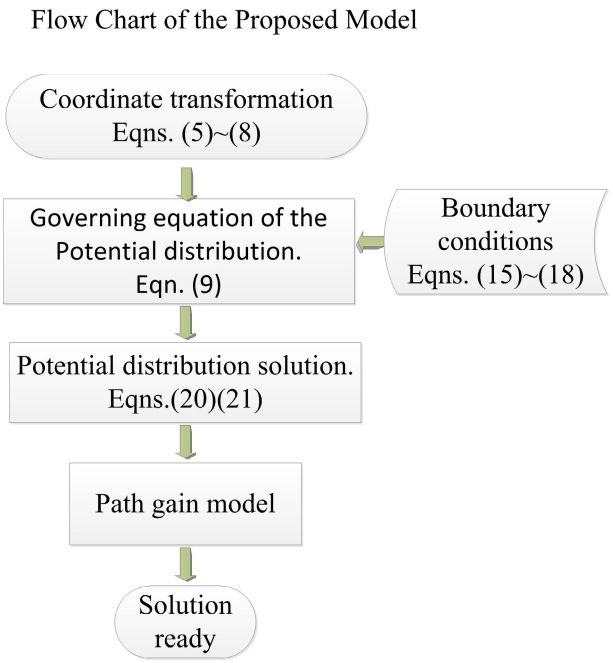

FIGURE 3. Flow chart of the proposed model.

$$Z(f,z) = \sum_{m=1}^{\infty} sin(\frac{m\pi z}{h}\sqrt{\widetilde{\sigma}_s(f)/\widetilde{\sigma}_{ls}(f)}); \quad (25)$$

III. VERIFICATION OF THE PROPOSED MODEL

A. VERIFICATION OF THE SAMPLES

To verify the rationality of the model, we recruited four volunteers (2 males, 2 females) aged 20-26 and measured the signal path-gain in their bodies at various distances, d. These volunteers were healthy and had no implantable electronic devices. The limbs were selected as the effective area for experimental verification. In order to demonstrate the experiment, we chose 40 mm × 40 mm physiotherapeutic electrodes for sending and detecting the signals. These electrodes are generally used in clinical medicine experiments and therapy. They can be stuck onto the human limbs and steadily transmit the signals. Before placing the electrodes, for ensuring good connectivity between the body surfaces and the detecting electrodes, the dead skin and dust on the limbs must be removed by wiping and cleaning several times with alcohol cotton paper. A calibrated network analyzer set (Agilent 4395A network/Spectrum/Impedance analyzer) was selected for measuring the signal path-gain. To avoid inaccuracy due to the common-ground of the instruments, we chose a set of differential probes (Agilent Technologies 1141A Differential Probe) for connection with the human limbs, as shown in Figure 4 and Figure 9, then input the current signal with a carrier signal of 1 kHz-1 MHz to measure the signal path-gain within the range, 1 kHz-1 MHz.

We then measured the geometric parameters of the human body. As human limbs may be approximated by a multilayer cylindrical volume conductor, to estimate each layer of the tissue radius more accurately, we precisely measured the arm circumferences at the signal source and at testing point, the wrist perimeters, and the body heights and weights. These data were listed in Table 1 to Table 2.

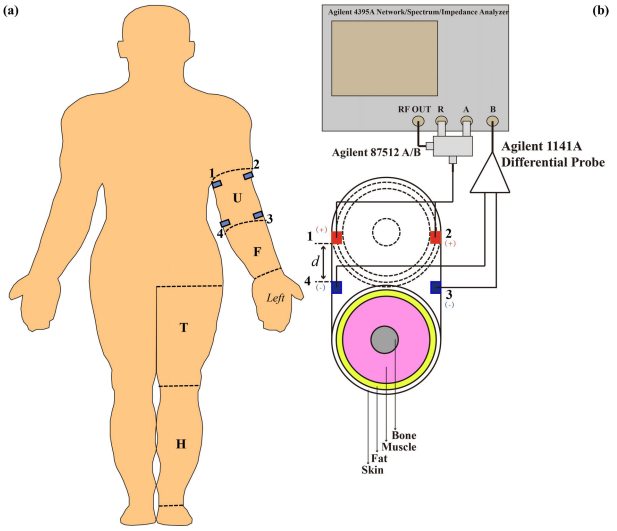

FIGURE 4. Schematic of the parallel verification.

TABLE 1. Samples body parameters.

Samples ID	Gender	Height (mm)	Mass (kg)	Wrist Cir (mm)	BMI
01	male	1710	64	206	21.9
02	male	1690	55	164	19.3
03	female	1620	49	151	18.7
04	female	1720	67	181	22.6

ID: Identity, Cir: Circumference, BMI: Body Mass Index

TABLE 2. Experiment point circumference.

Samples ID	Cir[source] (mm)	Cir[d=20 mm] (mm)	Cir[d=60 mm] (mm)
01	280	278	270
02	245	230	228
03	240	228	220
04	310	270	255

Cir: Circumference

B. TISSUE STRUCTURE PARAMETERS

In previous studies [30], [31], [42], the tissue parameters are basically obtained by means of equal scaling. This method is simple and easy to obtain. However, there are also some problems. Due to individual differences, the data obtained by standard scaling is inevitably too ideal, and it is difficult to reflect the influence of individual differences. To solve this problem, we propose to use CT technology to obtain human tissue structure parameters.

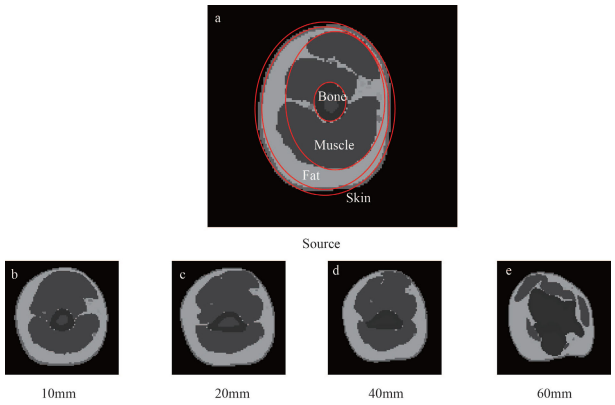

FIGURE 5. Geometric data of one left arm by CT scan.

TABLE 3. Samples tissue geometric parameters abstracted (approximate cylinder).

Tissue	01	02	03	04
Bone(20 mm)	21.8	15.38	16.18	22.69
Muscle(20 mm)	38.21	33.29	31.89	40.51
Fat(20 mm)	43.43	36.88	36.68	45.21
Skin(20 mm)	44.41	37.78	37.26	46.15
Bone(60 mm)	25.85	16.78	17.68	23.99
Muscle(60 mm)	38.11	33.79	32.89	40.51
Fat(60 mm)	42.78	36.66	35.62	43.98
Skin(60 mm)	43.77	37.64	36.60	44.96

First, we selected four healthy persons' arms as the measurement objects. After marked, the arms were scanned by CT (Siemens Somatom Sensation16 CT Scanner) to obtain the tissue geometric data (shown in Figure 5). By measuring the area, we can get the overall area of the arm section, bone area, muscle area and fat area. By abstracting each area into a circle, we can get the radius of each sample and each kind of tissue as shown in table 3. Using the parameters in Table 3, we can verify the consistency of the model more accurately.

Because this paper focus on verifying the performances of the two models with isotropic and anisotropic muscles under the same geometric parameters, estimation difference of the geometric parameters will not produce an effect on verification of the contrast test. Besides, because bone, skin and fat are all isotropic in the two models, they have the same electrical parameter; only the muscle layer is given electrical parameters in different forms.

From the above Geometric parameters, the radii (r_s) of the various organs in the multilayer volume conductor are obtained; after r_s and the human tissue parameters are substituted into equations (20) and (21), the signal path-gain from the isotropic and anisotropic model calculations can be derived within the range, 1 kHz - 1 MHz.

C. IN-VIVO EXPERIMENTS TO DETERMINE THE TISSUE CHARACTERISTICS

As the electric property of muscular tissue is significantly different in the transverse and parallel directions [34], transverse and parallel experiments need to be designed for model verification.

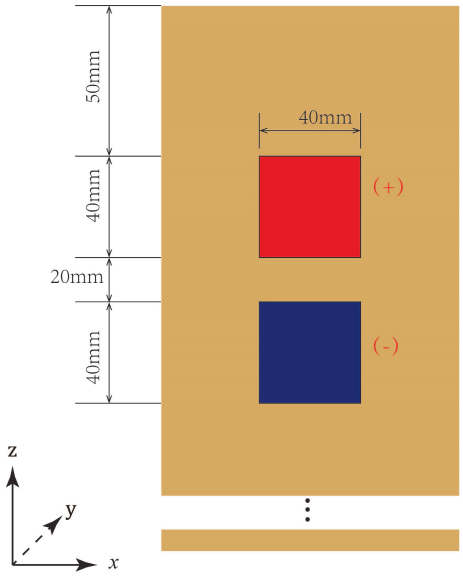

FIGURE 6. Current distribution (current density is the total current over the electrode area. The red and blue squares are for positive and negative electrodes, respectively).

1) PARALLEL VERIFICATION

For the parallel direction verification of the model, two positive electrodes were placed on the same side of the arm for signal transmitting and receiving while two negative electrodes were placed on the other side of the arm. The distance between the internal flanges of the two electrodes of the same side, d, was 20 mm. The transmitting electrodes were distributed symmetrically relative to the central point. See Figure 4 for the detailed design. The current signal, $\vec{J}_{nt}(f, \theta, z)$, inputting to the transmitting electrodes, can be expressed as follows:

$$\vec{J}_{nt}(f, \theta, z) = \begin{cases} \vec{J} & if\ 50\ mm < z < 90\ mm \\ 0 & otherwise \\ -\vec{J} & if\ 110\ mm < z < 150\ mm \end{cases} \quad 0 < \theta < 2\pi \tag{26}$$

where $\vec{J} = I/S$, S is the area of the electrode and I is the input current intensity (A) (shown in Figure 6).

In the experiment, after a sinusoidal current signal of 0 dBm is input to the transmitting electrode, a potential difference is produced due to the coupling between the electrodes and the human tissues; the coupling potential difference is called the coupling potential on the electrodes, indicated by $\varphi_{sL}(f, r, \theta, z)$, where $\varphi_{sL}(f, r, \theta, z)_{Anisotropic}$ and $\varphi_{sL}(f, r, \theta, z)_{Isotropic}$ are the *Anisotropic* and *Isotropic*, respectively. As the frequency, f, changes, the human-tissue conductivity properties between the positive and negative electrodes at the transmitting and receiving terminals vary accordingly; the coupling potential between the transmitting

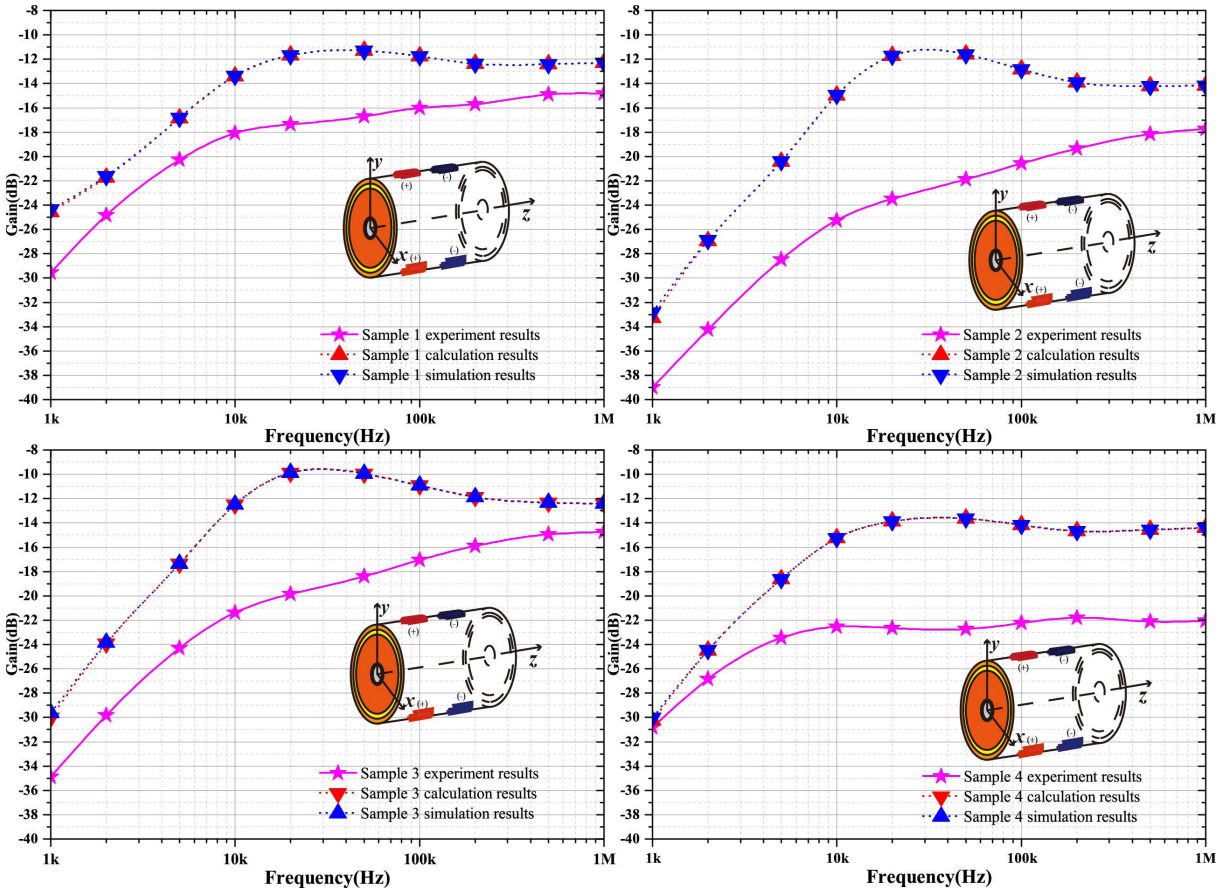

FIGURE 7. Parallel verification results (the transmitting electrodes and receiving electrodes are symmetrical, relative to the center).

and receiving terminals can be expressed as $\varphi_{sL}(f, r, \theta, z)_{TX}$ and $\varphi_{sL}(f, r, \theta, z)_{RX}$, respectively. The path-gain expression can be derived as (22).

When d is constant, $Gain(f, r, \theta, z)$ can be obtained for a different frequency, f. In order to verify the rationality of the model, we selected four experimental samples to conduct the same experiment and verified the rationality of the model by comparing the $Gain(f, r, \theta, z)$ from the experiments and the $Gain(f, r, \theta, z)$ from the analytical solution model calculation. In the process of verification, to demonstrate the accuracy of the model solution, we utilized the geometrical and electric parameters applied in the analytical solution model to build a numerical solution model; we then verified the accuracy of the analytical solution model by computing the signal gain, $Gain(f, r, \theta, z)$, when the distance, d, was the same as that in the analytical solution model. The results are shown in Figure 7.

Figure 7 shows the results of the numerical and analytical solution models for different experimental samples, at different carrier frequencies, f. By contrasting the calculation result of the analytical solution model based on the sample parameters, with the simulation result of the numerical solution model, it is concluded that the result of the analytical solution is consistent with that of the numerical solution; therefore, the analytical solution is correct. By comparing the analytical solution, the numerical solution, and the experimental results, it was determined that although there is certain error between the variation tendencies of the experimental results and the calculation results of the model solution, the overall variation tendency of the model is consistent. The variation tendency is also shown in Figure 7. Based on the research results of S. Gabriel [35], as the frequency, f, increases, the conductivity (Table 4 and Table 5) of the human tissues, $\sigma_s(f)$, increases, whereas, the Relative permittivity (Table 4 and Table 5), $\varepsilon_s(f)$, decreases. Therefore, the resistance between the transmitting and receiving electrodes continuously decreases and the capacitance constantly increases. As the electrical conductivity of a channel continuously improves, the capacitance effect becomes increasingly obvious.

Figure 8 shows the error between the analytical or numerical solution calculation results and experimental results, for different samples within the range, 1 kHz-1 MHz. It can be seen that the error between the numerical solution model calculation results and the experimental results and that between the analytical solution model calculation results are almost the same. This is because the parameters used in the numerical solution model and in the analytical solution model are the same and the calculation results of the two models are almost consistent; hence, the errors of the two models are nearly

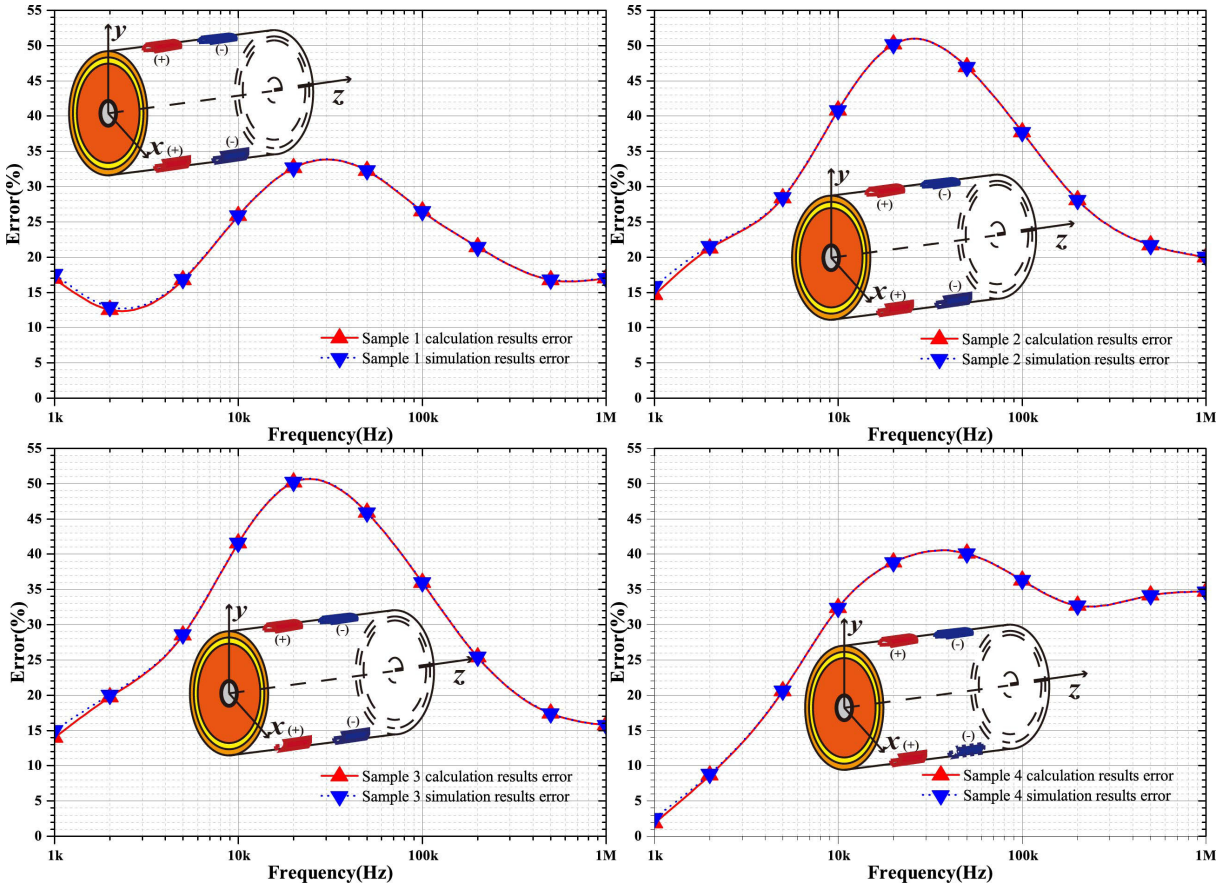

FIGURE 8. Parallel verification errors(the transmitting electrodes and receiving electrodes are symmetrical, relative to the center).

the same. As the sample tissue structures are different, in the model calculation, the sample parameters of the models can be obtained only by estimation; thus, the sample and model results vary to a certain extent.

2) TRANSVERSE VERIFICATION

For the transverse verification of the models, we placed the positive and negative signal-transmitting electrodes on both sides of the arm. The electrode configuration is the same as that in the parallel verification, the only change is in the transmitting and receiving methods. The detailed design is shown in Figure 9. The current signal, $\vec{J}_{nt}(f, \theta, z)$, input to the transmitting electrodes, can be expressed as follows:

$$\vec{J}_{nt}(f, \theta, z) = \begin{cases} \vec{J} & if \ -\triangle < \theta < \triangle \\ 0 & otherwise \\ -\vec{J} & if \ \pi - \triangle < \theta < \pi + \triangle \end{cases} \quad (27)$$
$$50\ mm < z < 90\ mm$$

where $\vec{J} = I/S$, S is the area of an electrode and I is the input current intensity (A), $\triangle = W/2r_N$ and W is the electrode width.

In order to ensure the quasi-static characteristics of the system, in the two groups of experiments, we input a current signal of 0 dBm within the range 1 kHz-1 MHz, through the transmitting electrodes.

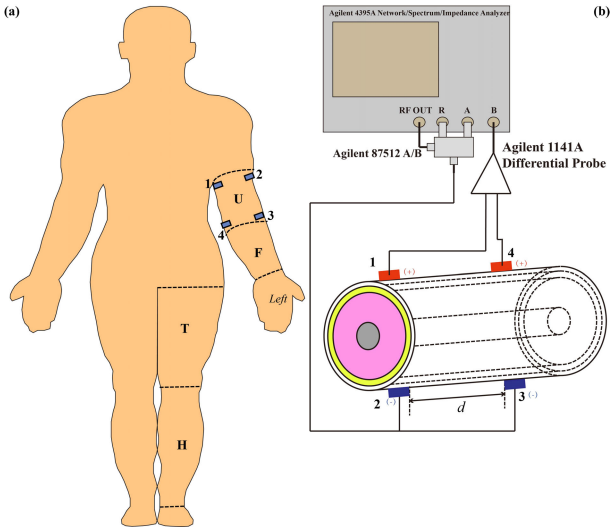

FIGURE 9. Schematic of the transverse verification.

Figure 10 depicts the results of the different sample anisotropic models, the isotropic model with muscular tissue characteristics, and the experiment. From the figure, it can

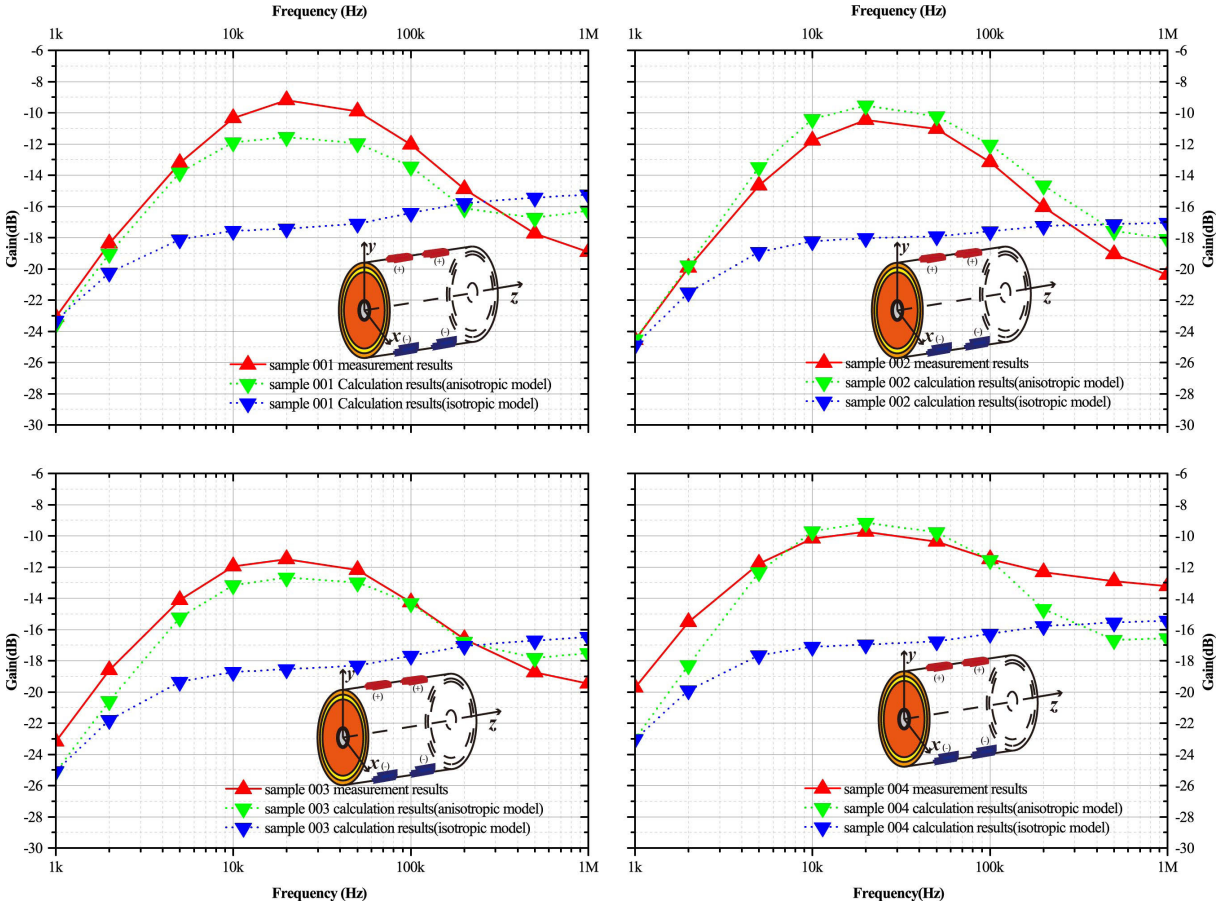

FIGURE 10. Transverse verification results (the transmitting electrodes are in parallel with the receiving electrodes).

be determined that when the communication frequency is within the range, 1 kHz-20 kHz, as the frequency increases, the path-gain of the channel continuously increases; the channel path-gain curve exhibits an increasing tendency with the increase in frequency; this characteristic exists both in the calculation result of the anisotropic model with muscular tissue characteristics and in that of the isotropic model, but the characteristics of the former model are closer to the experimental result. When the communication frequency is within the range, 20 kHz-1 MHz, as the frequency increases, the path-gain of the channel decrease; the channel path-gain curve shows a declining tendency as the frequency increases. This characteristic of the calculation result of the anisotropic model with muscular tissue characteristics is almost the same as that of the experimental result; the isotropic model calculation result shows an increasing tendency, opposite to the experimental result and it conflicts with the actual variation tendency. It is obvious that the anisotropic model with muscular tissue characteristics better coincides with the actual situation.

Figure 11 shows the error between the calculation results of different-sample anisotropic models with muscular tissue characteristics or that between the isotropic model and the experimental results within the frequency range, 1 kHz-1 MHz. It can be seen from the figure that the error between the calculation result of the isotropic model without muscular tissue characteristics and the experimental result is obviously larger than the error between the calculation result of the anisotropic model with muscular tissue characteristics and the experimental result. From the overall analysis of the four samples, it can be concluded that the latter error may be controlled within 30%, whereas the former error may reach 90%; hence, the latter is an unsuccessful modeling. Therefore, the anisotropic model with muscular tissue characteristics is superior to the isotropic model without muscular tissue characteristics.

To further analyze the performance of the model, we obtained the average error and the maximum error between the calculated result and the experimental result within the frequency range of 1 kHz to 1 MHz, so as to analyze the performance of the model (Figure 12). The data shown by pillar without grids in Figure 12 are the error analysis of isotropic model and experimental results, while the data shown by pillar with grids is the error analysis of anisotropic model and experimental results. It can be seen from the Figure 12 that, in the comparison analysis of the four samples, the anisotropic model with tissue characteristics are better than the isotropic model in terms of both the average

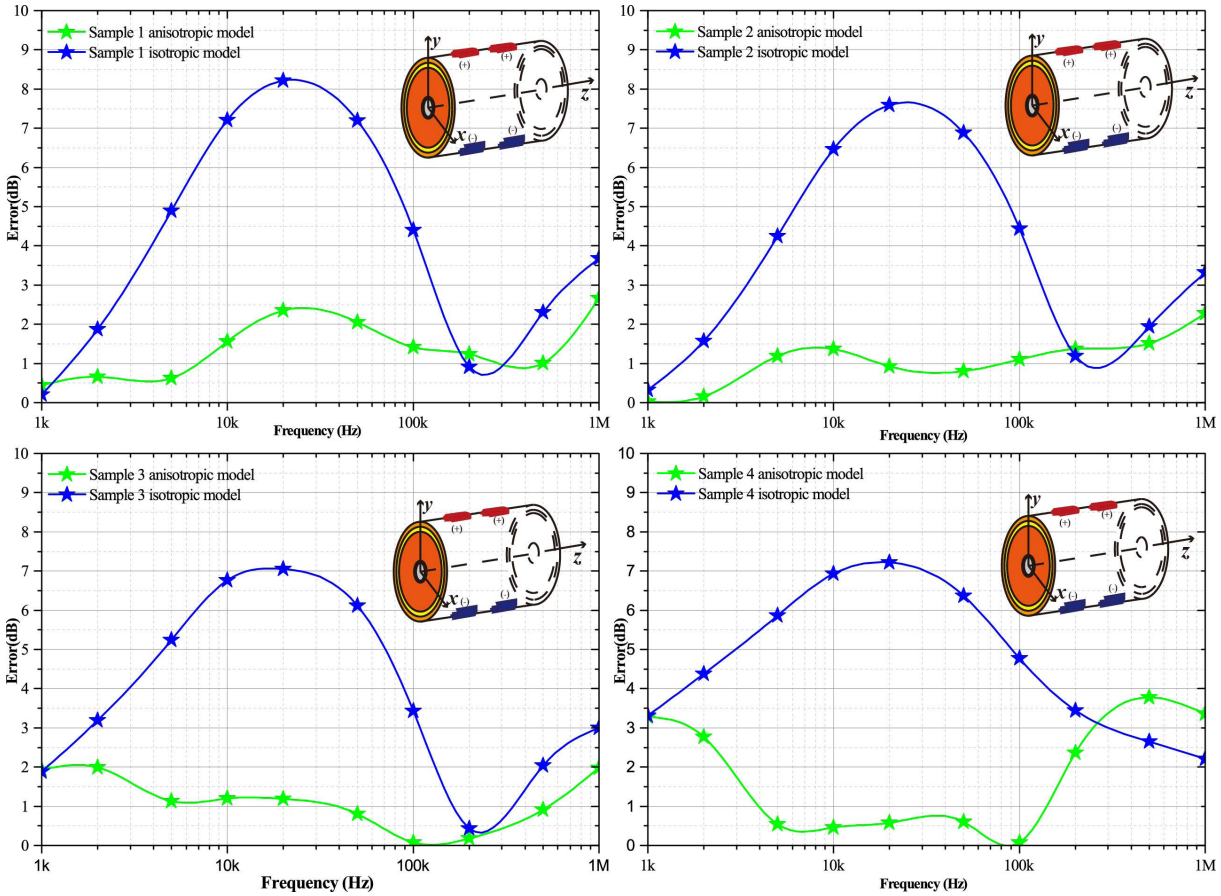

FIGURE 11. Transverse verification errors (the transmitting electrodes are in parallel with the receiving electrodes).

error and the maximum error between the model result and the experimental result.

IV. BEST COMMUNICATION BANDWIDTH

In the wearable medical communication system, the optimal communication band will directly determine the communication performance of the channel. In order to study the optimal communication frequency of the galvanic coupling human-body communication within the frequency range of 1 kHz to 1 MHz, we selected 50 healthy persons (25 males, 25 females) aged between 16 to 65 years old as the subjects of this experiment. They were voluntary, and the experiments were introduced to them in detail before the experiment. They were fully familiar with the experiment process and safety issues.

Since the actual communication is mainly the transverse communication, this experiment aims to measure channel gain when the z-axial distance changes. In the first measurement, the communication distance between the electrodes is 20 mm; afterwards the communication distance between electrodes is increased by an electrode width (40 mm) in each measurement. Because the effect of the human joints on channel communication has not yet been analyzed in this study, in this measurement, the maximum communication distance between electrodes was set as 100 mm. Among 25 samples, the channel gain with the communication distances of 20 mm (Figure 13(a)), 60 mm (Figure 13(b)) and 100 mm (Figure 13(c)) were measured. By analyzing three sets of experiments, we found that the optimal communication frequency band of human arm was 10 kHz to 50 kHz. Within this frequency band, the channel gain is the largest, and the mean deviation of samples is less than 2dB (Figure 13(d)), which is very beneficial to signal transmission in human body.

In order to study the change of channel gain with the increase of the communication distance, the average gain value at 20 kHz in Figure 13(d) was selected as the research object. The variation trend curve of path gain (Figure 13(e)) and fitting parameters of the fitting curve (Figure 13(f)) were obtained by linear fitting. It can be seen from Figure 13(e) that the fitting curve is consistent with the measured value. Meanwhile, by analyzing the fitting curve, we can also conclude that channel gain shows a linear decreasing trend with the increase of the channel distance.

V. DISCUSSION

In this study, after the simplification of the human limb tissue distribution, a multilayer analytical model is obtained. The simplified cylinder has a simple geometrical structure;

TABLE 4. Channel model tissue parameters (isotropic).

	Frequency (HZ)	Conductivity σ(S/m)	Relative permittivity ε_r
Bone	1k	2.00e-2	2.70e3
	10k	2.00e-2	5.20e2
	100k	2.10e-2	2.30e2
	1M	2.40e-2	1.4e2
Bone Cortical	1k	2.02e-3	2.70e3
	10k	2.04e-3	5.22e2
	100k	2.08e-3	2.27e2
	1M	2.44e-3	1.45e2
Muscle	1k	3.20e-1	4.30e5
	10k	3.40e-1	2.60e4
	100k	3.60e-1	8.10e3
	1M	5.00e-1	1.80e3
Fat	1k	2.24e-2	2.41e4
	10k	2.38e-2	1.09e3
	100k	2.44e-2	9.29e1
	1M	2.51e-2	2.72e1
Dry Skin	1k	2.00e-4	1.14e3
	10k	2.04e-4	1.13e3
	100k	4.51e-4	1.12e3
	1M	1.32e-2	9.91e2

TABLE 5. Muscle tissue parameters (anisotropic).

	Frequency (HZ)	Conductivity		Relative permittivity	
		σ_t(S/m)	σ_l(S/m)	ε_{tr}	ε_{lr}
Bone	1k	2.00e-2	2.00e-2	2.70e3	2.70e3
	10k	2.00e-2	2.00e-2	5.20e2	5.20e2
	100k	2.10e-2	2.10e-2	2.30e2	2.30e2
	1M	2.40e-2	2.40e-2	1.4e2	1.4e2
Bone Cortical	1k	2.02e-3	2.02e-3	2.70e3	2.70e3
	10k	2.04e-3	2.04e-3	5.22e2	5.22e2
	100k	2.08e-3	2.08e-3	2.27e2	2.27e2
	1M	2.44e-3	2.44e-3	1.45e2	1.45e2
Muscle	1k	3.50e-2	5.54e-2	5.58e5	1.37e6
	10k	3.69e-2	5.75e-2	3.24e4	2.73e4
	100k	4.03e-2	5.81e-2	8.83e3	1.96e3
	1M	5.21e-2	5.87e-2	1.78e3	4.06e2
Fat	1k	2.24e-2	2.24e-2	2.41e4	2.41e4
	10k	2.38e-2	2.38e-2	1.09e3	1.09e3
	100k	2.44e-2	2.44e-2	9.29e1	9.29e1
	1M	2.51e-2	2.51e-2	2.72e1	2.72e1
Dry Skin	1k	2.00e-4	2.00e-4	1.14e3	1.14e3
	10k	2.04e-4	2.04e-4	1.13e3	1.13e3
	100k	4.51e-4	4.51e-4	1.12e3	1.12e3
	1M	1.32e-2	1.32e-2	9.91e2	9.91e2

therefore, it is suitable for building an analytical solution model. However, some of the geometrical properties of the human organs will be inevitably lost due to the simplification, causing inaccurate results (Figure 5). In future research work, we intend to reduce the error due to the geometrical simplification by repeating multiple times the same circumference

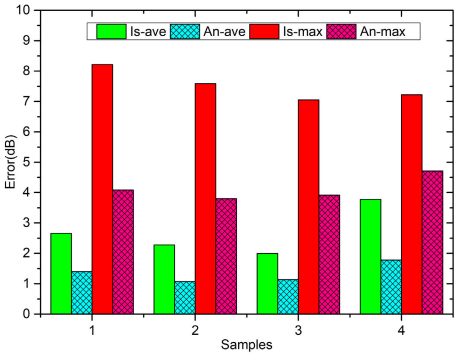

FIGURE 12. Model performance of anisotropic and isotropic models through transverse verification errors.

and then, averaging the measured values. From Figures (Figure 7, Figure 8, Figure 10, Figure 11 and Figure 12), it can be concluded that the anisotropic model with muscular tissue characteristics is better than the isotropic model without muscular tissue characteristics with respect to the curve variation tendency and the error between the model calculation results and the experimental results; the anisotropic model with muscular tissue characteristics is more accurate than the isotropic model without muscular tissue characteristics. The model precision is considerably improved by up to 200%, which is a significant breakthrough. However, there still exist errors in this model, with the maximum being 30%. This is caused by a series of modeling assumptions such as the geometric simplification and the quasi-static approximation.

In this paper, the characteristics of tissue anisotropy in the surface communication channel are discussed, and the consistency of the model is verified by experimentation. In the implantable communication channel, tissue characteristics also exist, but due to the limitations of current experimental conditions, this has not been verified. In the future, we will further design the implantable communication channel to verify the consistency of the model.

Figure 13 shows the measurement results of the human arm, the optimal communication frequency band and the fitting path gain model. In the actual communication system, wearable devices are more commonly used in the chest cavity and human legs. Whether these parts have the same properties and whether the fitting model is effective still need to be further verified. In addition, all measurement in this experiment was carried out in the static state of human body. In the dynamic state of human body, the effects of channel properties and motion noise on the channel need to be further studied.

The galvanic coupling intra-body communication is widely concerned in modern medicine because of its low communication frequency, very small radiation, stable transmission and long transmission distance, which can avoid signal leakage and lays a foundation for the security of signal transmission. In the research of channel transmission, in order to understand the transmission mechanism of signal in

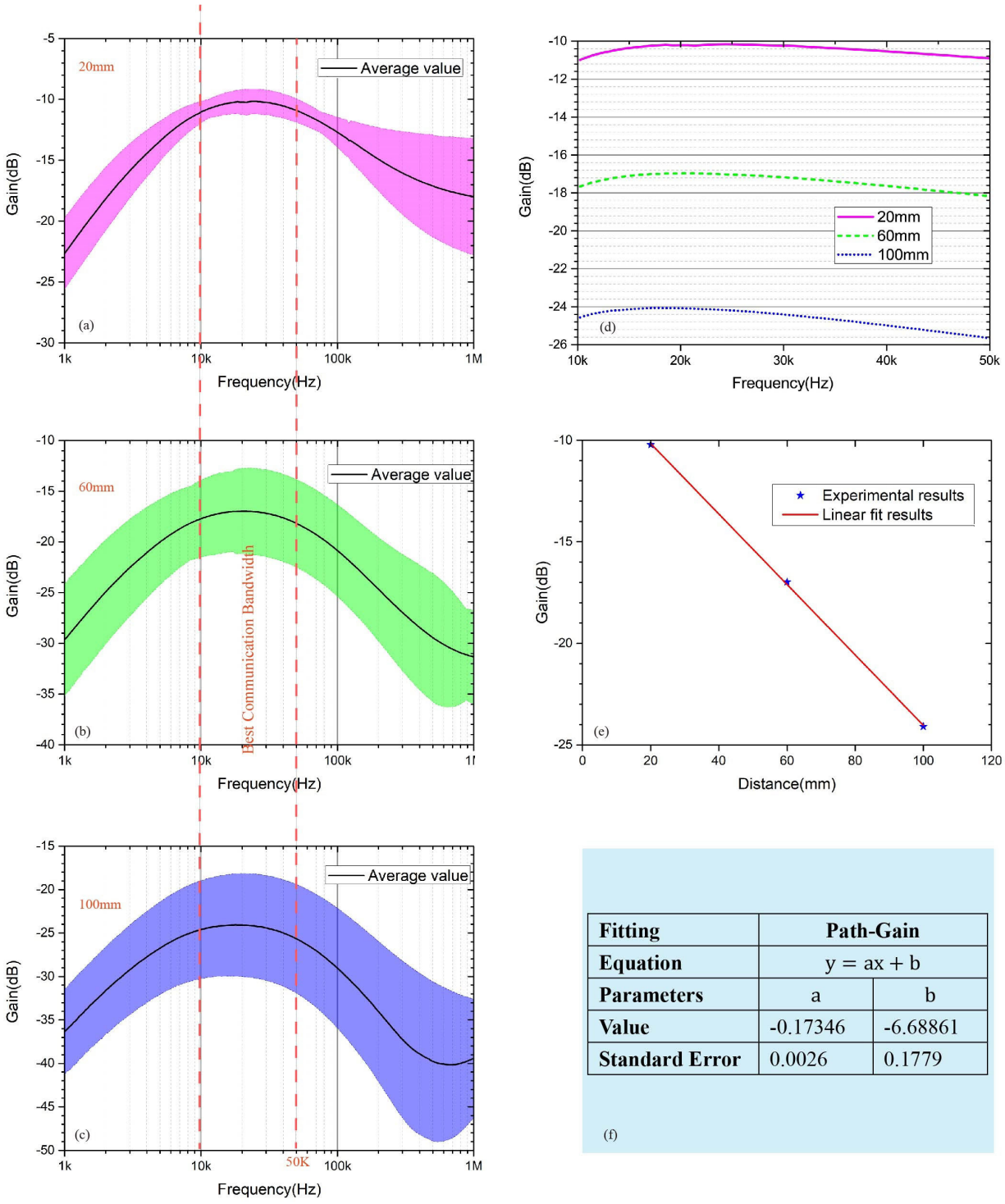

Fitting	Path-Gain	
Equation	y = ax + b	
Parameters	a	b
Value	-0.17346	-6.68861
Standard Error	0.0026	0.1779

(f)

FIGURE 13. Best communication bandwidth.

channel more accurately, researchers usually analyze its characteristics by establishing channel models. In modeling, human tissues are usually reduced to isotropy in order to meet the needs of the model and simplify the solution. In this way, the influence of tissue characteristics on the channel will be neglected. This will inevitably lead to the difference between the model result and the experimental result, especially the difference caused by tissue characteristics. In future research, we will continue to analyze the influence of other tissue characteristics on the channel.

VI. FUTURE WORKS

Although the muscle fiber tissue characteristics were added to the model, the model results are in good agreement with the experimental results. Meanwhile, the optimal communication frequency band of the system is found by analyzing the sample data. However, the following problems still need further study.

- 1) When the model was established, only the axial connectivity was considered, and the influence of joint on the model was not considered. In the future, we will further consider establishing the channel model with joint characteristics.
- 2) In the verification of the channel model introduced in this paper, we only considered verifying the simple cylinders such as limbs. As the human thoracic cavity is a more complex geometry, whether such simplification is reasonable or not will be verified by further experimentation and the model will also be modified in the future.
- 3) In the verification experiment, only quasi-static scenarios were considered. In the motion state, the consistency of the model needs further study.
- 4) By designing an actual communication system, the channel characteristics (such as channel capacity, signal-to-noise ratio, and bit error rate) of this method in the biomedical engineering will be verified.

VII. CONCLUSION

To reduce the model error and improve its precision, a channel modeling method with human muscular tissue characteristics was proposed in this study. In this method, Maxwell's equations were the governing equation and a galvanic-coupling human-body communication channel model with human tissue characteristics was built in the cylindrical coordinate system. By establishing a numerical solution model with the same parameters and deriving its solution, the solution was proved to be correct. The result verifies the modeling method effectively. By comparing the calculation results and experimental data, we found that the maximum error of the channel model with muscular tissue characteristics in the sample experiment was controlled below 30%, whereas the error of the isotropic model without muscular tissue characteristics reached 90%; hence, the precision of the channel model with human muscular tissue characteristics is significantly improved. The calculation result of the channel model with human muscular tissue characteristics was consistent with the experimental result, with respect to the variation tendency. Although the isotropic model without human muscular tissue has the same characteristics within the range, 1-10 kHz, it is opposite to the experimental result in the frequency range, 20 kHz-1 MHz and does not conform with the experimental result. Therefore, the channel model with human muscular tissue characteristics can present the signal path-gain in the frequency domain more accurately. At last, in order to study the optimal communication frequency of the galvanic coupling human-body communication within the frequency range of 1 kHz to 1 MHz, we selected 50 healthy persons (25 males, 25 females) aged between 16 to 65 years old as the subjects of this experiment. By the experiments, we found that the optimal communication frequency band of the human arm is 10 kHz to 50 kHz. Within this frequency band, the channel gain is the largest, and the mean deviation of samples is less than 2dB.

REFERENCES

[1] F. Sufi, Q. Fang, I. Khalil, and S. S. Mahmoud, "Novel methods of faster cardiovascular diagnosis in wireless telecardiology," *IEEE J. Sel. Areas Commun.*, vol. 27, no. 4, pp. 537–552, May 2009.

[2] Y. Gao and Y. Bando, "Carbon nanothermometer containing gallium," *Nature*, vol. 415, p. 599, Feb. 2002.

[3] S. Gabbe, J. Niebyl, J. Simpson, M. Landon, H. Galan, E. Jauniaux, D. Driscoll, V. Berghella, and W. Grobman, *Obstetrics: Normal and Problem Pregnancies*. Amsterdam, The Netherlands: Elsevier, 2012.

[4] J. J. N. Oats and S. Abraham, *Llewellyn-Jones Fundamentals of Obstetrics and Gynaecology*. Amsterdam, The Netherlands: Elsevier, 2016.

[5] S.-W. Chen and S.-C. Chao, "Compressed sensing technology-based spectral estimation of heart rate variability using the integral pulse frequency modulation model," *IEEE J. Biomed. Health Inform.*, vol. 18, no. 3, pp. 1081–1090, May 2014.

[6] Y. Kano, M. Yoshizawa, N. Sugita, M. Abe, N. Homma, A. Tanaka, T. Yamauchi, H. Miura, Y. Shiraishi, and T. Yambe, "Discrimination ability and reproducibility of a new index reflecting autonomic nervous function based on pulsatile amplitude of photoplethysmography," in *Proc. IEEE 36th Annu. Int. Conf. Eng. Med. Biol. Soc.*, Aug. 2014, pp. 1794–1800.

[7] Q. Liu, B. P. Yan, C.-M. Yu, Y.-T. Zhang, and C. C. Y. Poon, "Attenuation of systolic blood pressure and pulse transit time hysteresis during exercise and recovery in cardiovascular patients," *IEEE Trans. Biomed. Eng.*, vol. 61, no. 2, pp. 346–352, Feb. 2014.

[8] G. Vancoillie and R. Hoogenboom, "Responsive boronic acid-decorated (co)polymers: From glucose sensors to autonomous drug delivery," *Sensors*, vol. 16, no. 10, p. 1736, 2016.

[9] P.-J. Chen, S. Saati, R. Varma, M. S. Humayun, and Y.-C. Tai, "Wireless intraocular pressure sensing using microfabricated minimally invasive flexible-coiled LC sensor implant," *J. Microelectromech. Syst.*, vol. 19, no. 4, pp. 721–734, Aug. 2010.

[10] A. Natarajan, M. Motani, B. de Silva, K.-K. Yap, and K. C. Chua, "Investigating network architectures for body sensor networks," in *Proc. 1st ACM SIGMOBILE Int. Workshop Syst. Netw. Support Healthcare Assist. Living Environ. (HealthNet)*, New York, NY, USA, 2007, pp. 19–24.

[11] K. Liu, S. Li, X. Qie, Y. Du, R. Jiang, G. Lu, X. Mou, and G. Liu, "Analysis and investigation on lightning electromagnetic coupling effects of a dipole antenna for a wireless base station," *IEEE Trans. Electromagn. Compat.*, vol. 60, no. 6, pp. 1842–1849, Dec. 2018.

[12] N. Miura, D. Mizoguchi, T. Sakurai, and T. Kuroda, "Analysis and design of inductive coupling and transceiver circuit for inductive interchip wireless superconnect," *IEEE J. Solid-State Circuits*, vol. 40, no. 4, pp. 829–837, Apr. 2005.

[13] *Electromagnetic Compatibility and Radio Spectrum Matters (ERM); Radio Equipment in the Frequency Range 402 MHz to 405 MHz for Ultra-Low Power Active Medical Implants and Accessories, Part 1: Technical Characteristics, Including Electromagnetic Compatibility Requirements, and Test Methods*, Standard ETSI EN 301 839-1, European Telecommunications Standards Institute, 2002.

[14] T. G. Zimmerman, "Personal area networks (PAN): Near-field intra-body communication," M.S. thesis, MIT, Cambridge, MA, USA, 1995.

[15] T. G. Zimmerman, "Personal area networks: Near-field intrabody communication," *IBM Syst. J.*, vol. 35, no. 3.4, pp. 609–617, 1996.

[16] Y.-M. Gao, H.-F. Zhang, S. Lin, R.-X. Jiang, Z.-Y. Chen, Z. L. Vasić, M. I. Vai, M. Du, M. Cifrek, and S.-H. Pun, "Electrical exposure analysis of galvanic-coupled intra-body communication based on the empirical arm models," *BioMed. Eng. OnLine*, vol. 17, Jun. 2018, Art. no. 71.

[17] W. J. Tomlinson, S. Banou, C. Yu, M. Stojanovic, and K. R. Chowdhury, "Comprehensive survey of galvanic coupling and alternative intra-body communication technologies," *IEEE Commun. Surveys Tuts.*, vol. 21, no. 2, pp. 1145–1164, 2nd Quart., 2019.

[18] S. Kim and J. Ko, "IB-MAC: Transmission latency-aware MAC for electro-magnetic intra-body communications," *Sensors*, vol. 19, no. 2, 2019, Art. no. 341.
[19] J. Mao, H. Yang, Y. Lian, and B. Zhao, "A five-tissue-layer human body communication circuit model tunable to individual characteristics," *IEEE Trans. Biomed. Circuits Syst.*, vol. 12, no. 2, pp. 303–312, Apr. 2018.
[20] S. Zhang, S.-H. Pun, P. U. Mak, Y. P. Qin, Y. H. Liu, Y. M. Gao, and M. I. Vai, "Experimental verifications of low frequency path gain *(PG)* channel modeling for implantable medical device (IMD)," *IEEE Access*, vol. 7, pp. 11934–11945, 2019.
[21] S. Maity, M. He, M. Nath, D. Das, B. Chatterjee, and S. Sen, "Bio-physical modeling, characterization, and optimization of electro-quasistatic human body communication," *IEEE Trans. Biomed. Eng.*, vol. 66, no. 6, pp. 1791–1802, Jun. 2019.
[22] D. Das, S. Maity, B. Chatterjee, and S. Sen, "Enabling covert body area network using electro-quasistatic human body communication," *Sci. Rep.*, vol. 9, Mar. 2019, Art. no. 4160.
[23] J. Xiang, Y. Dong, X. Xue, and H. Xiong, "Electronics of a wearable ECG with level crossing sampling and human body communication," *IEEE Trans. Biomed. Circuits Syst.*, vol. 13, no. 1, pp. 68–79, Feb. 2019.
[24] Y. Nishida, K. Sasaki, K. Yamamoto, D. Muramatsu, and F. Koshiji, "Equivalent circuit model viewed from receiver side in human body communication," *IEEE Trans. Biomed. Circuits Syst.*, vol. 13, no. 4, pp. 746–755, Aug. 2019.
[25] S. Zhang, Y. P. Qin, P. U. Mak, S. H. Pun, and M. I. Vai, "Real-time medical monitoring system design based on intra-body communication," *J. Theor. Appl. Inf. Technol.*, vol. 47, no. 2, pp. 649–652, 2013.
[26] M. S. Wegmüller, "Intra-body communication (IBC) for biomedical sensor networks," Ph.D. dissertation, ETH, Zürich, Switzerland, 2007.
[27] K. Hachisuka, T. Takeda, Y. Terauchi, K. Sasaki, H. Hosaka, and K. Itao, "Intra-body data transmission for the personal area network," *Microsyst. Technol.*, vol. 11, nos. 8–10, pp. 1020–1027, 2005.
[28] K. Hachisuka, Y. Terauchi, Y. Kishi, K. Sasaki, T. Hirota, H. Hosaka, K. Fujii, M. Takahashi, and K. Ito, "Simplified circuit modeling and fabrication of intrabody communication devices," *Sens. Actuators A, Phys.*, vols. 130–131, pp. 322–330, Aug. 2006.
[29] M. S. Wegmueller, A. Kuhn, J. Froehlich, M. Oberle, N. Felber, N. Kuster, and W. Fichtner, "An attempt to model the human body as a communication channel," *IEEE Trans. Biomed. Eng.*, vol. 54, no. 10, pp. 1851–1857, Oct. 2007.
[30] X. M. Chen, P. U. Mak, S. H. Pun, Y. M. Gao, C.-T. Lam, M. I. Vai, and M. Du, "Study of channel characteristics for galvanic-type intra-body communication based on a transfer function from a quasi-static field model," *Sensors*, vol. 12, no. 12, pp. 16433–16450, 2012.
[31] S. H. Pun, Y. M. Gao, P. U. Mak, M. I. Vai, and M. Du, "Quasi-static modeling of human limb for intra-body communications with experiments," *IEEE Trans. Inf. Technol Biomed.*, vol. 15, no. 6, pp. 870–876, Nov. 2011.
[32] L. A. Geddes and L. E. Baker, "The specific resistance of biological material—A compendium of data for the biomedical engineer and physiologist," *Med. Biol. Eng.*, vol. 5, pp. 271–293, May 1967.
[33] G. V. Dimitrov and N. A. Dimitrova, "Extracellular potential field of a single striated muscle fibre immersed in anisotropic volume conductor, " *Electroencephalogr. Clin. Neurophysiol.*, vol. 4, pp. 423–436, Oct./Dec. 1974.
[34] F. L. H. Gielen, W. Wallinga-de Jonge, and K. L. Boon, "Electrical conductivity of skeletal muscle tissue: Experimental results from different muscles *in vivo*," *Med. Biol. Eng. Comput.*, vol. 22, pp. 569–577, Nov. 1984.
[35] S. Gabriel, R. Lau, and C. Gabriel, "The dielectric properties of biological tissues: II. Measurements in the frequency range 10 Hz to 20 GHz," *Phys. Med. Biol.*, vol. 41, no. 11, p. 2251, 1996.
[36] A. Heringa, D. F. Stegeman, G. J. H. Uijen, and J. P. C. De Weerd, "Solution Methods of Electrical Field Problems in Physiology," *IEEE Trans. Biomed. Eng.*, vol. BME-29, no. 1, pp. 34–42, Jan. 1982.
[37] R. Plonsey and D. B. Heppner, "Considerations of quasi-stationarity in electrophysiological systems," *Bull. Math. Biol.*, vol. 29, no. 4, pp. 657–664, 1967.
[38] R. Plonsey, *The Biomedical Engineering Handbook*, J. D. Bronzino, Ed. Boca Raton, FL, USA: CRC Press, 2000.
[39] J. Malmivuo and R. Plonsey, *Bioelectromagnetism*. New York, NY, USA: Oxford Univ. Press, 1995.
[40] J. M. Felício, C. A. Fernandes, and J. R. Costa, "Wideband implantable antenna for body-area high data rate impulse radio communication," *IEEE Trans. Antennas Propag.*, vol. 64, no. 5, pp. 1932–1940, May 2016.
[41] S. Zhang, S. H. Pun, P. U. Mak, Y.-P. Qin, Y.-H. Liu, and M. I. Vai, "Communication channel modeling of human forearm with muscle fiber tissue characteristics," *Technol. Health Care*, vol. 24, no. 5, pp. 681–687, 2016.
[42] H. B. Lim, D. Baumann, and E.-P. Li, "A human body model for efficient numerical characterization of uwb signal propagation in wireless body area networks," *IEEE Trans. Biomed. Eng.*, vol. 58, no. 3, pp. 689–697, Mar. 2011.

SHUANG ZHANG (S'15–M'19–SM'19) received the B.S. degree in mathematics and applied mathematics from Neijiang Normal University, Neijiang, China, in 2007, the M.S. degree in control engineering from the Institute of Optics and Electronics, Chinese Academy of Sciences, Chengdu, and the Ph.D. degree in electrical and electronic engineers from the University of Macau, Macau, China, in 2019.

He has been an Associate Professor with the College of Computer Science and AI and a Senior Engineer with the BeiDou and Wisdom Medical Doctor Workstation, Neijiang Normal University. He has been holding a Postdoctoral position at the School of Life Science and Technology, University of Electronic Science and Technology of China (UESTC). His current research interests include human body communication, digital signal processing, body sensor networks, and neuromodulation.

YI HE LIU (M'19) received the Ph.D. degree in applied mathematics from Sichuan University, Chengdu, China, in 2005. Since 2009, he has been involved in research in the areas of intra-body communications.

He is currently a Professor with the College of Computer Science, Neijiang Normal University.

YU PING QIN received the B.S. degree in mathematics and applied mathematics from Neijiang Normal University, Neijiang, China, in 2007, and the M.S. degree in probability theory and mathematical statistics from Sichuan Normal University, in 2011.

She has been an Associate Professor with the College of Computer Science, Neijiang Normal University. Her current research interests include human body communication, digital signal processing, and digital image processing.

JIANG MING KUANG received the B.S. degree in mechanical design and manufacturing from Northwest Polytechnic University, Xi 'an, China, in 1999, and the M.S. degree in mechanical and electronic engineering from the Huazhong University of Science and Technology, Wuhan, China, in 2002. He is currently a Teacher with Neijiang Normal University, China. His current research interests include electromechanical control and signal processing.

JI NING YANG received the B.S. degree in mathematics and applied mathematics from Leshan Normal University, Leshan, China, in 2015. He is currently pursuing the M.S. degree with the Chengdu University of Information Technology, Chengdu, China.

He is currently a Teacher with Neijiang Normal University, Sichuan, China. His current research interest includes signal processing.

JIA WEN LI received the master's degree with the Faculty of Science and Technology, University of Macau, Macau, China, in 2015, where he is currently pursuing the Ph.D. degree in electrical and computer engineering.

His current research interests include electroencephalography (EEG) signals analysis, affective computing, and human body communication.

JIU JIANG WANG (S'15–M'19–SM'19) received the B.S. degree in microelectronic circuits and systems from the Beijing Institute of Technology, Beijing, China, in 1991, the M.S. degree in semiconductor devices and microelectronic from the Institute of Semiconductors, Chinese Academy of Sciences, Beijing, in 1994, and the Ph.D. degree from the University of Macau, Macau, China, in 2019.

He was a system design engineer with an IC company. He has been an Associate Professor with the College of Computer Science, Neijiang Normal University, Sichuan, China. His current research interests include modeling and fabrication of CMUT devices, human body communication, body sensor networks, and neuromodulation.

TAO ZHANG received the B.S. and M.S. degrees from Shanghai Jiao Tong University, Shanghai, China, in 1996 and 1999, respectively, and the Ph.D. degree in mechanical engineering from Florida State University, in 2004.

From 2005 to 2012, he was a Senior Scientist with the General Electric (GE) Global Research Center. Since 2012, he has been the Chief Technology Officer and the Vice President of Alltech Medical System in China. He is currently a Professor with the School of Life Science and Technology, University of Electronic Science and Technology of China (UESTC). He held over 20 patents. He has published over 30 technical articles. His research interests include the magnetic resonance imaging (MRI) system technologies and its clinical applications, MRI system hardware development, and the applications of MRI technique in neuroscience and brain research.

XUE MING ZOU received the M.S. degrees in physics from Oregon State University (OSU), Corvallis, OR, USA, in 1986, and the Ph.D. degree in bio-medical physics from the Massachusetts Institute of Technology, Cambridge, in 1990.

He is currently a Professor with the School of Life Science and Technology, University of Electronic Science and Technology of China (UESTC), and the Group Leader of the High-field Magnetic Resonance Brain Imaging Key Laboratory, Sichuan. He was the Founder, the President, and the CEO of USA Instruments which scratch to a number one in global market share in MRI coils, from 1993 to 2002. He also served as the Global Vice President and the General Manager of the Greater China Region of MR Business Division of GE. In 2005, he founded the AllTech Medical Systems Company Ltd., a China Corporation, Chengdu, where he was the President. His research interests include MRI system physics, advanced medical diagnostic imaging applications, and big data in medical imaging.